ELEMENTA
Science of the Anthropocene

Kazemi, R, et al. 2021. Investigating methane emissions from geologic microseepage in Western New York State, United States. *Elem Sci Anth*, 9: 1. DOI: https://doi.org/10.1525/elementa.2020.00066

RESEARCH ARTICLE

Investigating methane emissions from geologic microseepage in Western New York State, United States

Roxana Kazemi[1,*], William Schlageter[1], Benjamin Hmiel[1,2], Thomas S. Weber[1], Lee T. Murray[1], and Vasilii V. Petrenko[1]

Methane is a powerful greenhouse gas and a key player in atmospheric chemistry. Important uncertainties remain in the global atmospheric methane budget, with natural geologic emissions being one of the particularly uncertain terms. In recent bottom-up studies, geologic emissions have been estimated to comprise up to 10% of the global budget (40–60 Teragrams of methane per year, Tg CH_4 yr^{-1}). In contrast, top-down constraints from ^{14}C of methane in preindustrial air extracted from ice cores indicate that the geologic methane source is approximately an order of magnitude lower. Recent bottom-up inventories propose microseepage (diffuse low-level flux of methane through soils over large areas) as the largest single component of the geologic methane flux. In this study, we present new measurements of methane microseepage from the Appalachian Basin (Western New York State) and compare these with prior microseepage measurements from other regions and with predicted values from the most recent bottom-up inventory. Our results show lower microseepage values than most prior data sets and indicate that positive microseepage fluxes in this region are not as widespread as previously assumed. A statistical analysis of our results indicates that mean microseepage flux in this region has very likely been overestimated by the bottom-up inventory, even though our measurements more likely than not underestimate the true mean flux. However, this is a small data set from a single region and as such cannot be used to evaluate the validity of the microseepage emissions inventory as a whole. Instead, the results demonstrate the need for a more extensive network of direct geologic emission measurements in support of improved bottom-up inventories.

Keywords: Microseepage, Geologic methane, Appalachian Basin, Methane budget

Background and motivation

Methane is the second most important anthropogenic greenhouse gas, with a global warming potential of 28–32 over a 100-year period (Etminan et al., 2016). Natural methane emissions are dominated by wetlands, with smaller contributions from freshwater, ocean, geologic sources, and wildfires, while anthropogenic emissions are from agriculture, waste, fossil fuels, biomass, and biofuel burning (Saunois et al., 2020). Atmospheric methane is primarily removed by reaction with OH radicals, with smaller contributions from stratospheric loss, reaction with chlorine, and removal by soil uptake (Saunois et al., 2020).

Geologic sources refer to methane that is naturally released from fossil hydrocarbon reservoirs both onshore and offshore and have been estimated by bottom-up approaches to contribute up to 10% of methane in the contemporary atmosphere (Etiope, 2015; Saunois et al., 2020). Anthropogenic fossil methane emissions arise from oil and gas production, coal mining, and natural gas distribution and use and are one of the largest and most uncertain terms in the global atmospheric methane budget (Saunois et al., 2016; Schwietzke et al., 2016; Hmiel et al., 2020; Saunois et al., 2020). Isotopic studies of atmospheric methane are useful for providing top-down constraints on the overall magnitude of anthropogenic fossil emissions. However, since both anthropogenic fossil and natural geologic methane emissions originate from the same reservoirs, emissions from these two categories are difficult to distinguish via isotopic measurements. In order to use top-down isotopic techniques to constrain anthropogenic fossil methane emissions and provide targets for global emission reductions, a reliable estimate of natural geologic methane emissions is essential.

Ice core records allow for the use of a top-down isotopic approach to estimate the magnitude of natural geologic emissions in the absence of anthropogenic fossil emissions. Several recent ice core studies used

[1] Department of Earth and Environmental Sciences, University of Rochester, Rochester, NY, USA

[2] Environmental Defense Fund, New York, NY, USA

* Corresponding author:
Email: rkazemi@u.rochester.edu

Table 1. Estimated natural geologic methane emissions from recent studies that used ice core ^{14}C-CH_4 measurements compared with recent bottom-up estimates. DOI: https://doi.org/10.1525/elementa.2020.00066.t1

Study	Study Type	Estimated Geologic Emissions (Tg CH_4 yr^{-1})
Petrenko et al. (2017)	Top-down ice core ^{14}C (last deglaciation)	<15.4
Hmiel et al. (2020)	Top-down ice core ^{14}C (preindustrial, early industrial)	<5.4
Dyonisius et al. (2020)	Top-down ice core ^{14}C (last deglaciation, early Holocene)	<19
Etiope (2015)	Bottom-up	45–76 (median 60)
Etiope et al. (2019)	Bottom-up	42.8–49.8

Table 2. Geologic CH_4 global bottom-up extrapolated emissions from Etiope et al. (2019). DOI: https://doi.org/10.1525/elementa.2020.00066.t2

Emission Category	CH_4 Extrapolated Emissions (Tg CH_4 yr^{-1})
Onshore seeps (including mud volcanoes and miniseepage)	8.1
Submarine seeps	>7
Microseepage	24
Geothermal manifestations	5.7
Total	42.8–49.8

measurements of carbon-14 of methane in trapped ancient air to suggest a low geologic contribution to the methane budget (**Table 1**; Petrenko et al., 2017; Dyonisius et al., 2020; Hmiel et al., 2020). These past measurements should be applicable today because natural geologic emissions are expected to change on very long (tectonic, glacial) timescales (Etiope et al., 2008). Conversely, bottom-up studies have estimated the geologic contribution as being an order of magnitude greater (**Table 1**; Etiope, 2015; Etiope et al., 2019). Further, it has recently been argued by Etiope and Schwietzke (2019) that ice core measurements of ethane (Nicewonger et al., 2016) and $\delta^{13}C$ of methane (Schwietzke et al., 2016) in the preindustrial atmosphere provide top-down estimates of the natural geologic methane source that are consistent with the bottom-up estimates in **Table 1**. However, ethane and $\delta^{13}C$ of methane in the preindustrial atmosphere may not be capable of providing strong constraints on geologic methane emissions because of uncertainties involved in the interpretation of these proxies (Hmiel et al., 2020). Thus, there is currently a strong disagreement among estimates of geologic methane emissions that appear difficult to reconcile (Etiope & Schwietzke, 2019).

Onshore natural geologic methane sources include volcanoes, mud volcanoes, oil and gas seeps (macroseeps), microseepage, and geothermal seeps (Etiope, 2015). Microseepage, which is postulated to be the largest component of geologic emissions (**Table 2**), is defined as the widespread diffuse flux of geologic methane through the soil at intensities up to hundreds of mg CH_4 m^{-2} day^{-1} that is generally not associated with a macroseep (Etiope et al., 2011; Etiope, 2015; Etiope et al., 2019). Miniseepage is another category of geologic methane seepage that can manifest as a diffuse flux, although at higher intensities (hundreds to thousands of mg CH_4 m^{-2} day^{-1}); it is usually, but not always, associated with a larger macroseep (Etiope et al., 2011; Etiope, 2015).

The previously published global microseepage data set (Etiope et al., 2019) contains 1,509 measurements from 10 hydrocarbon basins (**Table 3**; Klusman et al., 2000; Klusman, 2003; Etiope, 2005; Klusman, 2005; Etiope et al., 2006; LT Environmental, 2007; Tang et al., 2007; Etiope & Klusman, 2010; Tang et al., 2010, 2017; Etiope et al., 2019). Sampled areas are primarily in Western United States, Italy, and Northwest China, with a few additional measurements in Romania and Greece, leaving most of the world's hydrocarbon basins unrepresented in the global data set.

Etiope et al. (2019) provided the most recent estimates of methane emissions from microseepage in a globally gridded format. In this statistical-model estimate, all petroleum-forming areas (approximately 10% of global land surface) were considered capable of microseepage emissions. Each $0.05^\circ \times 0.05^\circ$ grid cell's microseepage estimate was based on predictive geologic indicators such as faulting, earthquakes, and known gas seeps. In the Etiope et al. (2019) study, statistics of the 1,509 individual measurements of microseepage (**Table 3**) were examined to establish four microseepage levels; a seepage level was then assigned to each grid cell based on the presence or absence of predictive geologic indicators (**Table 4**). Etiope et al. (2019) randomly assigned 54% of Level 1 cells to zero seepage values based on past measurement statistics. However, in this study, the cells with no predicted microseepage are defined as Level 0.

Here we present new measurements of microseepage in the Appalachian Basin from Western New York State, United States. The presented measurements are directly compared to the Etiope et al. (2019) predictions of microseepage fluxes for this region, with the ultimate goal of improving the bottom-up statistical model estimates of microseepage. Western New York State is an excellent location for this type of study since it is underlain by gas and oil-rich shale layers and has several known natural gas macroseeps as well as miniseepage (Etiope et al., 2013; Schimmelmann et al., 2018). Etiope et al. (2019) predicted high microseepage fluxes for this region (**Figure 1**), and

Table 3. Hydrocarbon basins with prior published CH_4 microseepage measurements. DOI: https://doi.org/10.1525/elementa.2020.00066.t3

Hydrocarbon Basin	Studies	Study Region	Number of Measurements	Average Microseepage Flux (mg CH_4 m^{-2} day^{-1})	Median Microseepage Flux (mg CH_4 m^{-2} day^{-1})
Tarim	Tang et al. (2007, 2010, 2017)	Northwest China	100	11.6	1.80
Alps	Etiope (2005), Etiope et al. (2019), Etiope and Klusman (2010), Sciarra et al. (2013)	Italy	372	231.0	5.72
Pannonian-Transylvanian	Etiope (2005)	Central Romania	5	23.5	11.0
Peloponnesus	Etiope et al. (2006, 2019)	Kalamata, Greece	27	7.66	4.0
Powder River	Klusman et al., (2000), Klusman (2005)	Wyoming, United States	198	0.0977	0.129
Railroad Valley	Etiope et al. (2019), Klusman et al. (2000)	Nevada, United States	124	–0.0230	0.110
Denver-Julesurg	Etiope et al. (2019), Klusman et al. (2000)	Colorado, United States	252	0.459	0.655
Piceance	Klusman et al., (2000), Klusman (2003)	Colorado, United States	306	11.6	0.0593
Raton	LT Environmental (2007)	Colorado, United States	60	1,290	576
Gulf Coast	Etiope et al. (2019)	Texas, United States	65	0.246	-0.767
$N = 9$	$N = 12$	$N = 8$	$N = 1{,}509$		
Appalachian	This study	Western New York State, United States	47	–0.606	–0.202

Table 4. Microseepage flux values assigned to cells of each level in Etiope et al. (2019). DOI: https://doi.org/10.1525/elementa.2020.00066.t4

Etiope et al. (2019): Microseepage Levels	Level 0	Level 1	Level 2	Level 3	Level 4
Microseepage flux value (mg CH_4 m^{-2} day^{-1})	0	1.3	31.1	101	493.54
Geologic seepage indicators associated with emission levels in Etiope et al. (2019)	None	None	Faults or earthquakes	Faults plus earthquakes, or oil seeps, or gas-bearing springs	Gas macroseeps or mud volcanoes

Ciotoli et al. (2020) also predicted high methane seepage favorability in this area. Prior soil gas measurements in this area also indicated that microseepage to the atmosphere is likely occurring along some fault zones (Fountain & Jacobi, 2000; Jacobi, 2002). While microseepage is postulated to be the largest component of natural geologic CH_4 emissions in Western New York State (Etiope et al., 2019), we are not aware of any prior flux chamber measurements of microseepage flux to the atmosphere in this region or elsewhere in the Appalachian Basin. In the Etiope et al. (2019) microseepage gridding, Level 0, Level 1, and Level 4 microseepage fine grid (0.05° latitude × 0.05° longitude) cells are all present within the Western New York State region. Since local geologic data sets were not considered in the Etiope et al. (2019) study, some cells that should have been classified as Level 2 or 3 due to the presence of faulting, recent earthquakes, or both were instead assigned to Level 0 or Level 1 by the Etiope et al. (2019) model. In this study, the sampled grid cells with these indicators are corrected to Level 2 where indicated (Table S1).

Methods

Sampling site selection

Natural gas macroseeps, faulting, and recent seismic events are considered as predictive factors for microseepage; seepage is also more likely to manifest in local topographic lows where valleys cut through gas-bearing geologic strata (Etiope, 2015; Etiope et al., 2019). To select sampling areas, an ArcGIS map of each of these parameters alongside the fine-grid emission estimates from Etiope et al. (2019) was generated (**Figure 2**).

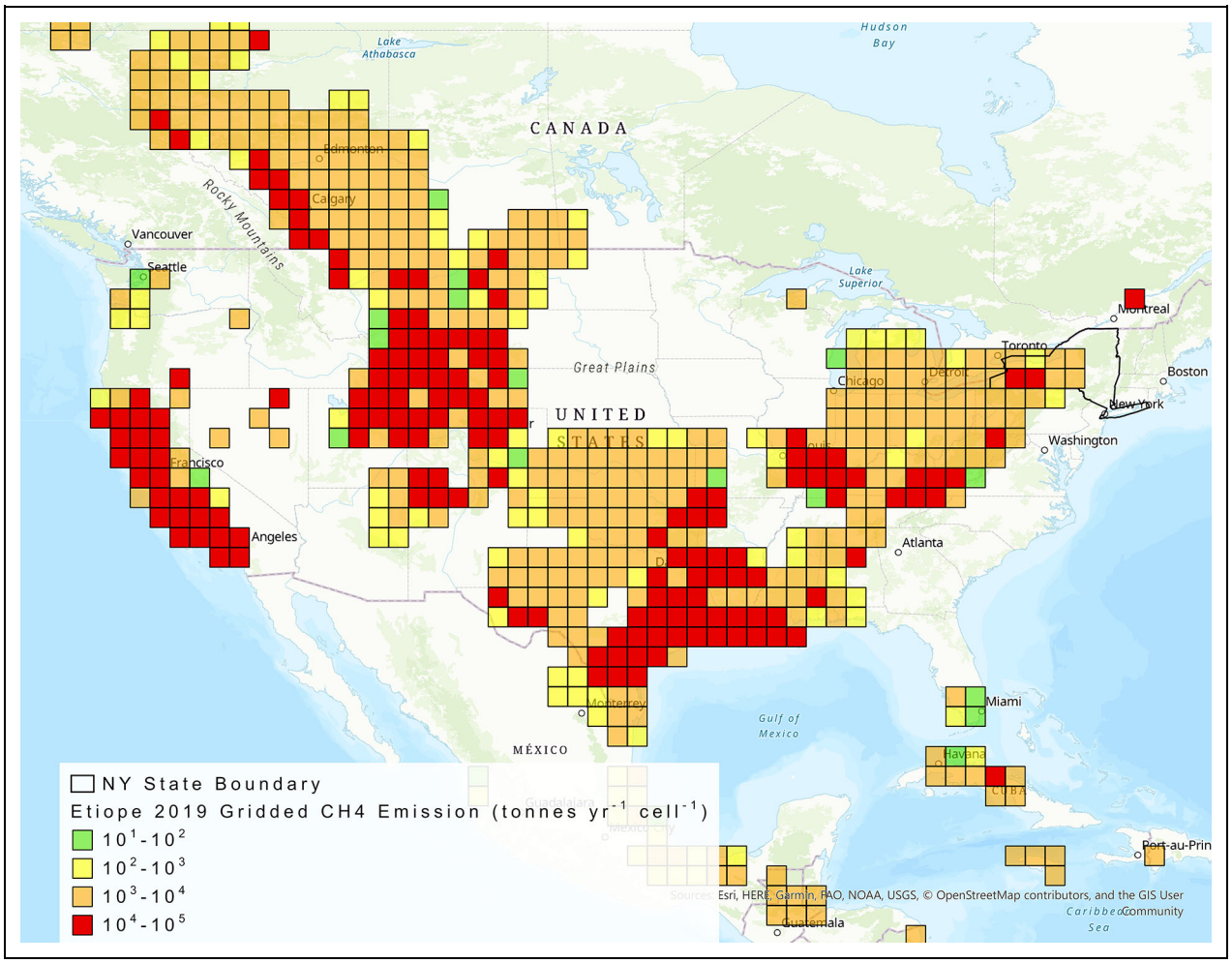

Figure 1. A map of coarsely gridded (1° latitude × 1° longitude) methane microseepage emission estimates for the United States from data published in Etiope et al. (2019). The two red high-emission cells located in Western New York State are the focus of this study. DOI: https://doi.org/10.1525/elementa.2020.00066.f1

Sampling locations were chosen to include the full range of the Etiope et al. (2019) predicted seepage levels and geologic indicators with the intention of collecting a data set representative of microseepage variability in the Western New York State region (**Figure 2**; Tables S1 and S2). About a quarter of the measurements were collected in Level 4 cells with predicted high microseepage. Level 4 grid cells make up less than 1% of the total area in this region but are important to characterize because of their disproportionately large predicted contribution to overall microseepage emissions. Approximately 20% of the measurements were collected within 0.5 km of previously mapped fault lines (**Figure 2**). Five of the measurements were also collected within a ≈0.5 km stretch along a stream that encompasses a known macroseep and two miniseepage zones (Etiope et al., 2013), including a site within ≈8 m of the macroseep (sampling area e in **Figure 2** and **Tables 5**, S1 and S2). Due to the convenience in gaining access permits, all sampling was conducted within public parks. A 1-km buffer zone was adopted around known oil and gas wells, in which sampling was avoided. The buffer zone was intended to minimize any potential interference in the natural microseepage signal from oil and gas operations (Figure S1). Avoiding the buffer zone was possible in the majority of locations, but a few exceptions were made to allow sampling near features of high interest such as active seeps (Table S2). Within each area (denoted by letters on the map), local topographic lows, topographic highs, and intermediate elevation sites were sampled in an attempt to gain a representative view of the full range of microseepage variability.

Flux chamber design and procedure

A custom flux chamber was constructed based on the principles used in prior surface methane emission studies and similar to those used in previous microseepage studies (Klusman et al., 2000; Klusman, 2003, 2005; Etiope, 2005; Etiope et al., 2006; LT Environmental, 2007; Tang et al., 2007; Etiope & Klusman, 2010; Tang et al., 2010; Oertel et al., 2016; Tang et al., 2017; Elder et al., 2020). The apparatus, as depicted by **Figure 3**, uses a closed chamber in conjunction with a Los Gatos Research Portable Greenhouse Gas Analyzer (LGR Gas Analyzer) to measure the CH_4, CO_2, and H_2O vapor mole fractions over a set amount of time in the chamber for each sample. The flux chamber is a modified high-density polyethylene bucket with a lid

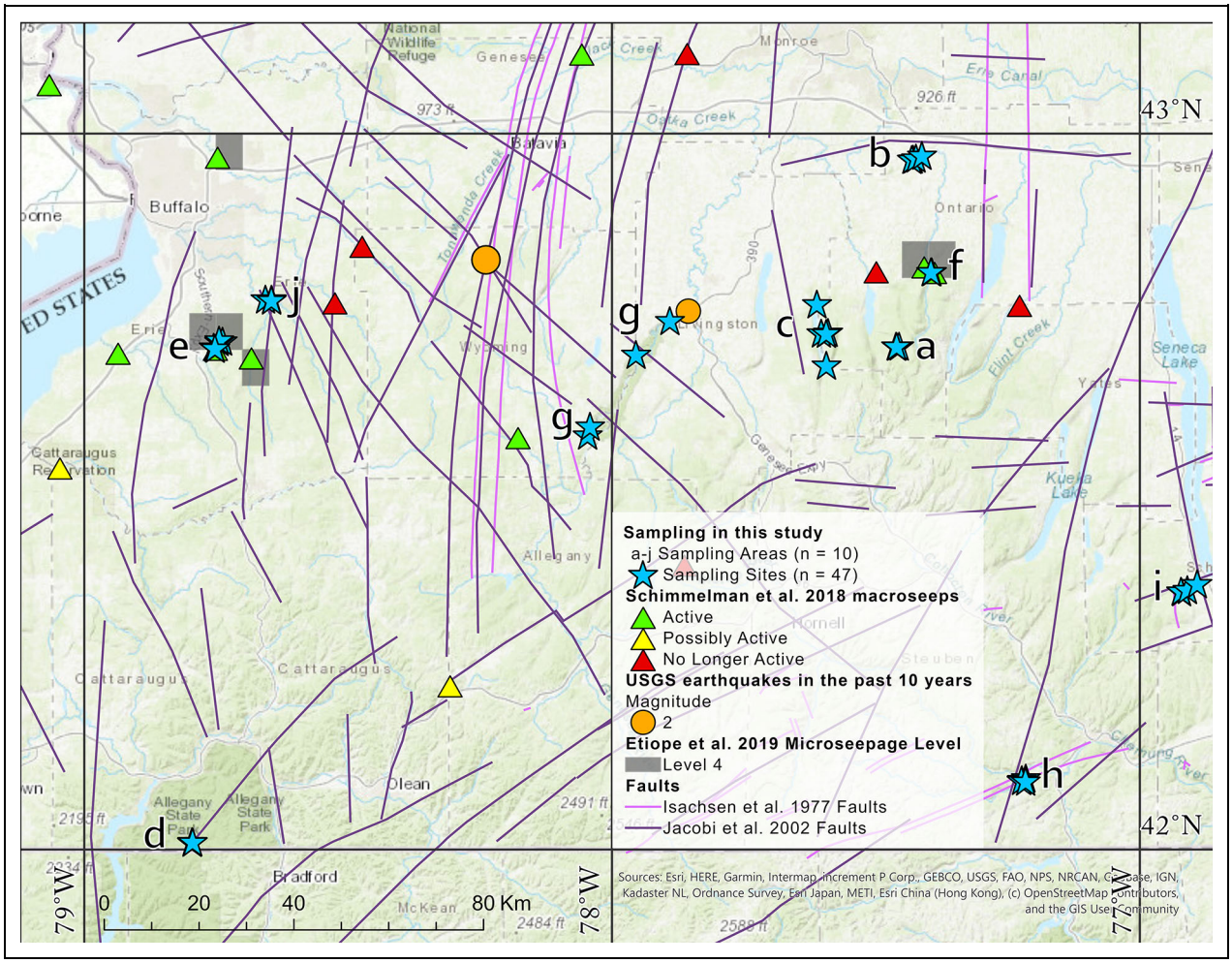

Figure 2. Map of the area of interest in Western New York State. The map showing faults (Isachsen & McKendree, 1977; Jacobi, 2002), recent earthquakes (U.S. Geological Survey, 2019), known gas seeps (Schimmelman et al., 2018), the fine-scale 0.05° × 0.05° grid of microseepage emission levels assigned by Etiope et al. (2019; only Level 4 is highlighted, as the rest of the cells in the region were randomly assigned between Level 1 and Level 0), the sampling sites, and the sampling areas based on the key in Table S1. Note that in sampling area e, the sampling site stars obscure an active seep; in area f, the sampling site stars also partially obscure two active seeps. DOI: https://doi.org/10.1525/elementa.2020.00066.f2

that seals with an o-ring, and quick-connect ports installed in the top which connect to the LGR Gas Analyzer through ¼″ outside diameter (OD) tubing (Synflex 1300). The flux chamber includes a vent (≈2 m of 1/16″ OD stainless steel tubing) to ensure pressure equilibration with ambient air.

During sampling, the bottom of the flux chamber is pushed into the soil, and the change in the methane mole fraction ($[CH_4]$) over time in the chamber can be used to calculate the soil CH_4 flux (Equation 1). Text S1 of the supplement provides further detail on calibration, flux detection, and blank testing with the system, and Figure S2 provides a photo of the sampling system setup in the field.

In addition to soil flux sample measurements, a dry standard gas from a 6-L Restek SilcoCan with a known $[CH_4]$ of 1.473 ± 0.007 μmol mol^{-1} was measured at the start and end of each sampling day to verify instrument performance and to check for any drift over the course of the day.

The sampling procedure is as follows. Prior to the first sample of the day, an initial standard gas measurement is taken over a 3-min interval. Once this is complete, the chamber is opened to the atmosphere to equilibrate with ambient air and then pushed approximately 2 cm into the soil surface. The LGR gas analyzer circulates air at approximately 450 standard cubic centimeters per minute (sccm) and measures the three greenhouse gas concentrations in the chamber over an approximately 10-min period. During this period, sampling site metrics are recorded such as wind speed, sample coordinates, elevation, soil temperature, chamber temperature, distance from significant features; a general description of the site is also recorded and photos are taken. When the measurement is complete, the Synflex lines are disconnected for transport and the LGR Gas Analyzer continues to measure ambient air en route in between sampling sites. After the final measurement of the day, another 3-min standard measurement is performed.

Table 5. Measured average CH_4 flux values compared to corresponding emission level estimates in Etiope et al. (2019). DOI: https://doi.org/10.1525/elementa.2020.00066.t5

Sampling Area(s) Key	Number of Samples	Assigned Seepage Level in Etiope et al. (2019)	Average Measured Flux (mg CH_4 m^{-2} day^{-1}) [a]	Estimated Microseepage (mg CH_4 m^{-2} day^{-1}) in Etiope et al. (2019)
a	6	Level 0/Level 1	−1.81 ± 0.608	0.598
b	4	Level 0/Level 1	−0.989 ± 0.820	0.598
c	6	Level 0/Level 1	−0.482 ± 0.303	0.598
a, b, c average	16	Level 0/Level 1	−1.10 ± 0.337	0.598
d	4	Level 2	−1.11 ± 0.541	31.1
g	4	Level 2	−0.306 ± 0.129	31.1
h	4	Level 2	−0.433 ± 0.439	31.1
i	4	Level 2	−0.448 ± 0.244	31.1
j	3	Level 2	−0.00763 ± 0.069	31.1
d, g, h, i, j average	19	Level 2	−0.484 ± 0.164	31.1
e	6	Level 4	−0.305 ± 0.181	493.54
f	3	Level 4	−0.0242 ± 0.0151	493.54
e, f average	9	Level 4	−0.212 ± 0.126	493.54

[a]Uncertainties represent the standard error of the mean.

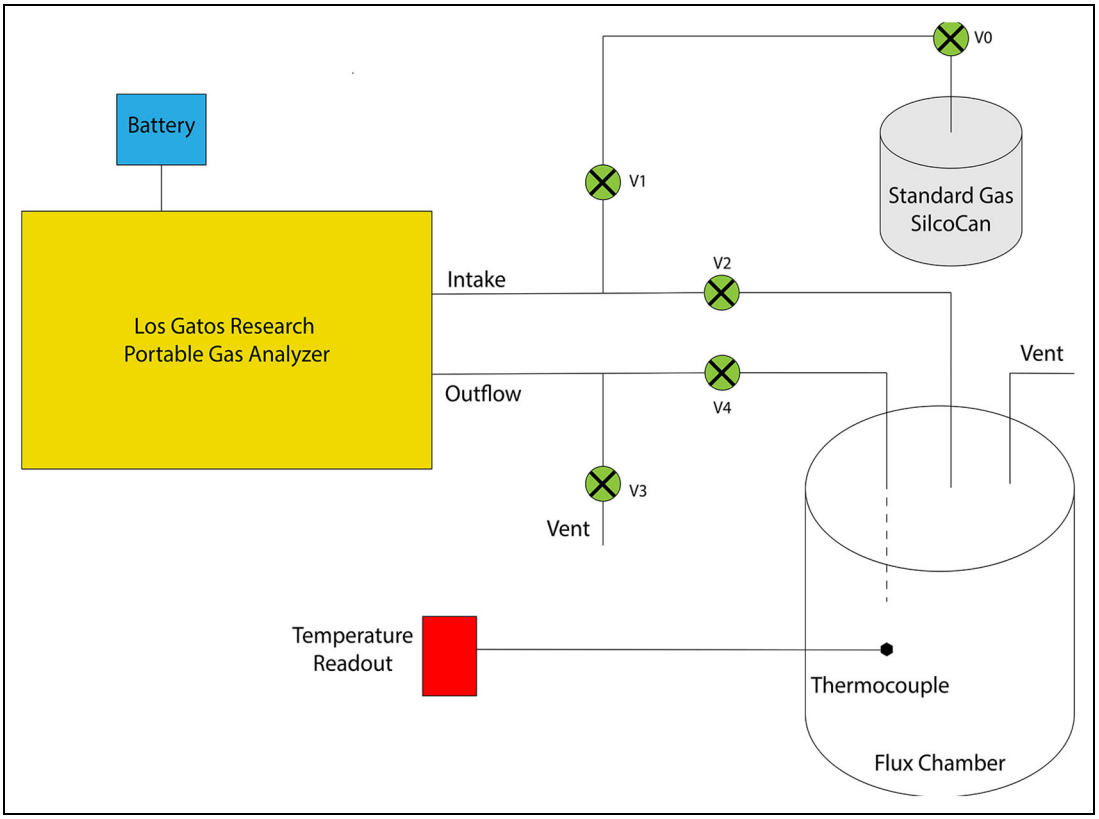

Figure 3. A schematic of the sampling system. During sampling, valves V1 and V3 are closed and V2 and V4 are open to constantly circulate air between the flux chamber and Los Gatos Research Portable Greenhouse Gas Analyzer. During standard gas measurement, V1 and V3 are open, and V2 and V4 are kept closed. DOI: https://doi.org/10.1525/elementa.2020.00066.f3

Data processing

After visiting each area, time series data were examined for data quality as described in supplement Text S2. The CH_4 flux for each site was calculated using a standardized MATLAB script and the following equation:

$$\text{flux} = \left(\frac{d[\text{CH}_4]}{dt}\frac{1,440\ \text{min}}{1\ \text{day}}\right)\left(\frac{V}{22.4\ \text{L mol}^{-1}}\frac{273\ \text{K}}{T}\frac{P}{1013\ \text{mbar}}\right)\left(\frac{16,040\ \text{mg CH}_4\text{mol}^{-1}}{A}\right) \quad (1)$$

Equation 1 is used to solve for sample flux. The resulting flux computed by Equation 1 is in units of mg CH_4 m^{-2} day^{-1}. $d[CH_4]/dt$ is the rate of $[CH_4]$ change in the chamber in mol mol^{-1} min^{-1}, V is the chamber volume in liters, T is the air temperature inside the chamber in K (average of T readings at start and end of flux measurement), A is the area of the opening at the bottom of the chamber (the effective flux area) in m^2, and P is the hourly ambient air pressure in mbar obtained from local weather stations.

To determine $d[CH_4]/dt$, the MATLAB linear regression function film was used over the full measurement time interval. This method also provides the standard error of the linear slope. Figure S7 provides an example of the linear $[CH_4]$ behavior during a typical sample measurement. To avoid artifacts in $d[CH_4]/dt$ associated with chamber placement and switching between chamber air and standard gas, the first and last minute of $[CH_4]$ measurements are excluded from the $d[CH_4]/dt$ analysis.

The uncertainties in each parameter in Equation 1 are propagated using standard techniques to determine the uncertainty in CH_4 flux. The largest sources of uncertainty are the chamber's volume calibration and, for some samples, $d[CH_4]/dt$.

The average flux for each area was compared to the Etiope et al. (2019) microseepage estimates (adjusted for seepage level reclassification if needed, as discussed above; **Table 5**). Because grid cells with no known geologic indicators were randomly assigned either Level 0 or Level 1 microseepage flux at a ratio of 54:46 in Etiope et al. (2019), the predicted flux of these cells was averaged to be 0.598 mg CH_4 m^{-2} day^{-1} and classified as a single low-flux group. Three samples with highly variable $d[CH_4]/dt$ (Table S2, Text S2) were excluded from further analyses in the main text, but included in the analysis in Figure S11 in the supplement; inclusion of these samples does not affect the study's conclusions.

Statistical analysis of how well our samples capture regional mean flux

A Monte Carlo statistical analysis was conducted to investigate the regional representativeness of the measurements in this study, given the potential for spatial and temporal patchiness in CH_4 microseepage. In this analysis, hundreds of thousands of synthetic microseepage flux distributions for our 1° × 2° main study region (depicted in **Figures 1** and **2**) were generated by drawing spatially (and in some tests also temporally) correlated random samples from a probability distribution fit to the microseepage flux data compilation from Etiope et al. (2019). The mean microseepage flux for each synthetic distribution was required to match the mean flux predicted by Etiope et al. (2019) for our 1° × 2° study region (≈4 mg CH_4 m^{-2} day^{-1}), but the fluxes vary from ≈–10 mg/m^2/day to ≈500 mg/m^2/day across spatiotemporal scales of 1–100 km and 1–180 days. These synthetic distributions were then sampled at the locations/times matching the actual field measurements in this study, and the mean microseepage flux for each synthetic set of samples was then computed. This yields the probability that the study data set underestimates the mean regional microseepage, and the probability of finding the mean of the study sample set if the Etiope et al. (2019) mean microseepage flux estimate is regionally representative. Full details of this analysis are given in Text S3 of the Supplement.

Results and discussion

The field measurements and calculated flux values for each sample are presented in Table S2. In **Table 5**, the average microseepage fluxes for each sampling area are compared to the Etiope et al. (2019) statistical model predictions.

All of the sampling areas yielded negative or negligible (within uncertainty of zero) average CH_4 fluxes; this is most likely due to the soil CH_4 sink. Negative flux values indicate that soil gas $[CH_4]$ is lower than atmospheric, which implies an absence of a positive geologic CH_4 flux to the atmosphere. We therefore interpret negative soil flux values as indications of zero geologic emissions to the atmosphere at those sites. While there is variability in fluxes measured within each area (Table S2), for the Level 2 areas, the Etiope et al. (2019) microseepage estimate (31.1 mg CH_4 m^{-2} day^{-1}) exceeds one standard deviation of all measured average microseepage values by more than an order of magnitude. For areas classified as Level 4, this discrepancy is three orders of magnitude.

Our measurements included multiple sampling sites in proximity of flux-predictive features such as macroseeps and faults (see Methods). Considering this, our results indicate that geologic CH_4 microseepage fluxes in this region are not ubiquitously associated with such features and suggest that the positive fluxes are not as widespread as assumed for this region by the Etiope et al. (2019) inventory. However, individual flux chamber measurements have a very limited spatial and temporal footprint; the number of measurements in this study is likewise relatively limited. The likely heterogeneity of geologic CH_4 microseepage emissions in space and time makes upscaling flux chamber measurements to a regional mean flux estimate inherently challenging. To further illustrate this point, despite the fact that all of our sampling areas in **Table 5** above yielded negative or negligible CH_4 fluxes, prior soil gas measurements (Fountain & Jacobi, 2000) at the southern margin of the Clarendon-Linden Fault system in Western New York State strongly suggested that at least some areas of positive fluxes exist in this region.

We used a statistical analysis (see Methods and Text S3 in the Supplement) to investigate how representative our

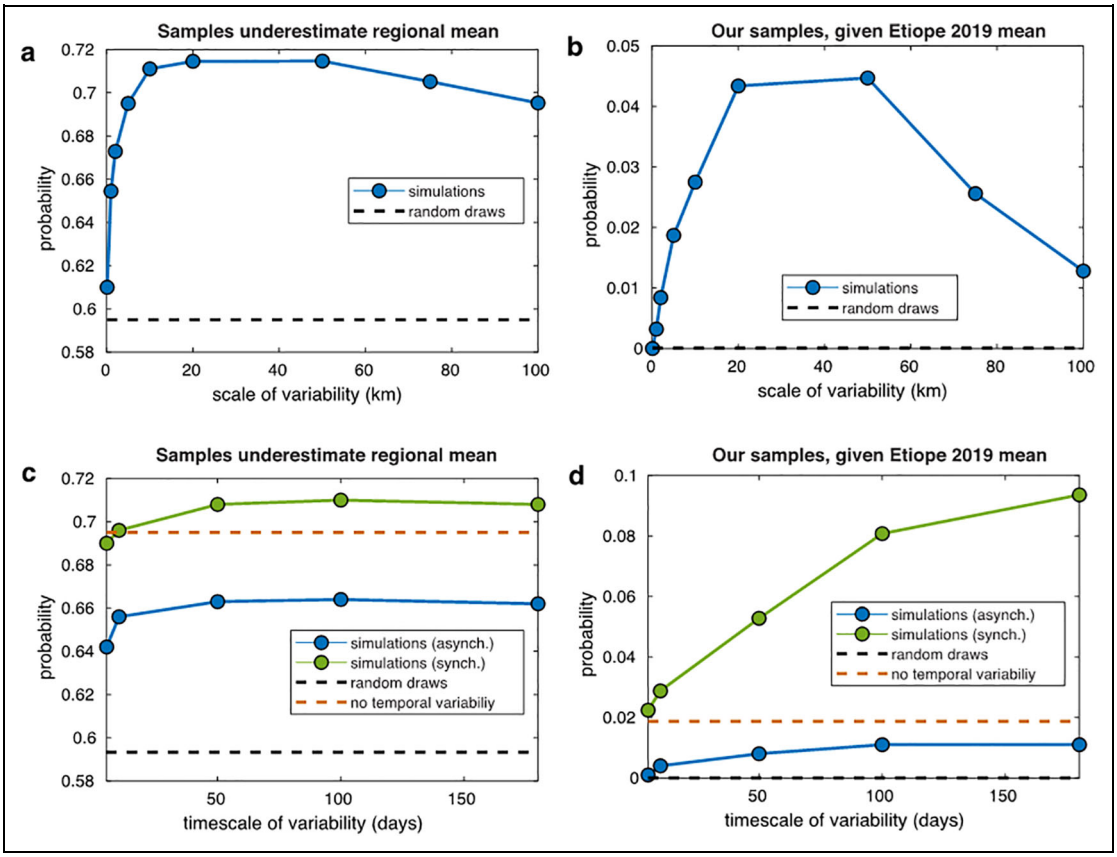

Figure 4. Results of the statistical analysis. The statistical analysis investigated the probability that our set of measurements underestimated the true regional mean CH_4 microseepage flux (panels a and c) and the probability of finding our measured mean CH_4 flux if the true mean flux is equal to the Etiope et al. (2019) prediction for this 1° × 2° region (≈4 mg CH_4 m^{-2} day^{-1}; panels b and d). For panels a and b, the synthetic flux distributions assumed no temporal variability in the flux. For results in panels c and d, temporal variability was assumed and the spatial scale of flux variability in the synthetic data was 5 km. In all cases, black dashed line shows the same probabilities if samples are drawn directly from the emissions probability distribution, rather than a synthetic data set with spatial and temporal structure. This represents the extreme scenario in which emissions are truly random in space and time. DOI: https://doi.org/10.1525/elementa.2020.00066.f4

limited measurements are of the true regional mean microseepage CH_4 flux. The results of this analysis (**Figure 4**) indicate that it is more likely than not (60%–72% probability) that our measurements underestimate mean microseepage in the region (28%–40% probability that our measurements overestimate the mean; **Figure 4a** and **c**). However, the analysis also indicates that it is highly improbable (<5% chance in most scenarios) that our set of measured fluxes (mean + *SE* ≈–0.47 mg CH_4 m^{-2} day^{-1}) could have been observed if the true regional mean microseepage CH_4 flux is as high as estimated by Etiope et al. (2019) (≈4 mg CH_4 m^{-2} day^{-1}; **Figure 4b** and **d**). The probability that our set of flux measurements could be made in a region with mean emissions of 4 mg CH_4 m^{-2} day^{-1} peaks for spatial variability scales of ≈20–50 km (**Figure 4b**). In these scenarios, relatively rare negative rates (Figure S12) would cluster into coherent features that could have been over-sampled by our clustered sampling strategy (**Figure 2**). For larger scales of variability, regions of high emissions would be "too hard to miss," and our sampling strategy is more likely to reflect the true regional mean (**Figure 4a**).

The probability that the regional mean predicted by Etiope et al. (2019) remains correct despite our lower measured rates also increases if the flux undergoes region-wide synchronous temporal variations, meaning we could have sampled only at times of anomalously low flux. However, this probability only exceeds 5% (reaching up to 10%) for synchronous temporal variability on relatively long time scales of 50 days or longer (**Figure 4d**). The only plausible driver of synchronous variability on these timescales would be seasonal flux changes due to the soil sink. However, most of our samples were collected during the fall and winter seasons, with relatively cold (but not frozen) soils when the soil CH_4 sink is relatively low, in principle allowing for relatively more geologic CH_4 flux to the atmosphere (see further discussion of this below). It is therefore not plausible that we sampled only during "low points" of the seasonal flux cycle. Ruling out these cases, our statistical analysis demonstrates with high confidence (>95%) that our measurements cannot be reconciled with a regional mean flux as high 4 mg CH_4 m^{-2} day^{-1}, making it very likely that Etiope et al. (2019) overestimated microseepage CH_4 flux in this region.

Flux chambers have a very limited footprint, and eddy covariance CH_4 measurements are not available in Western New York State for comparison with our results. Instead, we attempted to use satellite measurements to examine whether our flux chamber measurements are representative of microseepage CH_4 fluxes on larger spatial scales in this region. We aggregate column-average bias-corrected CH_4 mixing ratios from the TROPOspheric Monitoring Instrument (TROPOMI; Hu et al., 2018; Copernicus Sentinel-5P, 2019) over 8 × 8 km horizontal resolution using the recommended quality-control filters for a 2-year interval (May 2018–May 2020) that included the time interval of the flux chamber measurements (Sep 2019–Jan 2020); these results are shown in Supplementary Figure S14. The typical reported precision of the TROPOMI column-averaged CH_4 is 3 nmol mol^{-1}. Considering this precision and the mean near-surface wind speed in our study region, TROPOMI may in a best case scenario be able to detect intense CH_4 microseepage from clusters of two or more Level 4 fine grid cells in the Etiope et al. (2019) classification (at 494 mg CH_4 m^{-2} day^{-1}; see Supplementary Text S4). The examined TROPOMI data do not reveal positive CH_4 anomalies associated with Level 4 cells in our regions (cells containing active macroseeps; Figure S14). However, given the TROPOMI measurement precision of 3 nmol mol^{-1}, emissions of 494 mg CH_4 m^{-2} day^{-1} from these Level 4 fine grid cells cannot be conclusively ruled out (see Supplementary Text S4).

The mean and median CH_4 flux values for our entire data set (–0.62 and –0.20 mg CH_4 m^{-2} day^{-1}, respectively) are at the low end of such values when compared to prior microseepage data (**Table 3**). While the data sets from southern Europe and northwest China generally show much higher fluxes, the data sets from most Western U.S. locations are more similar to our measurements, with one of the regions (Nevada) also yielding a negative mean flux and one of the regions (Texas) yielding a median flux that is more negative than our result for Western New York State.

We propose four possible explanations for why our measurements show much lower microseepage flux values than many prior data sets and why the Etiope et al. (2019) model may have systematically overestimated microseepage fluxes in Western New York State. First, it is possible that for some of the prior data sets compiled by Etiope et al. (2019), the locations of microseepage measurements were biased toward high-seepage areas rather than representative of average fluxes. This also relates to our conclusion above that (at least for Western New York State) positive microseepage fluxes are not nearly as widespread as assumed by the Etiope et al. (2019) inventory. For example, the Raton Basin (Colorado, United States) measurements (LT Environmental, 2007) are the data sets with the highest measured fluxes, and the measurements were all taken within a few hundred meters of known macroseeps. It is not clear to us whether that set of measurements could even be classified as "microseepage" because Etiope (2015) classifies the soil emission "halo" surrounding a focused macroseep as "miniseepage" instead, reserving the term "microseepage" for fluxes that are independent of a macroseep. In contrast, our study was designed specifically to avoid bias toward either low- or high-seepage areas.

Second, it is possible that recent seismic activity within a basin plays a greater role in microseepage than the Etiope et al. (2019) model accounts for. The prior data sets that yielded relatively high mean microseepage fluxes are mainly from regions that are more seismically active than Western New York State (e.g., Italy; Schulte & Mooney, 2005; Incorporated Research Institutions for Seismology, 2021). Regions that are more similar to the Appalachian Basin in terms of seismic activity (e.g., Colorado, Wyoming, Texas) have yielded data sets with mean flux values more similar to ours.

Third, it may be possible that the lack of overpressure in the shale gas systems in most of the study region (e.g., Ryder, 2008) contributes to relatively low microseepage fluxes.

Fourth, the approach taken in the Etiope et al. (2019) statistical model for linking microseepage flux magnitude to predictive geologic features was qualitative in nature and did not attempt to quantitatively examine the relationship between flux and distance to the nearest fault or seep, for example. Such an approach is speculative and could result in large errors.

Our study was limited in the number of samples as well as in its spatial extent. It may be possible that the Western New York State region is anomalous in terms of microseepage; this is impossible to know without conducting further detailed sampling in multiple other regions. No conclusions could be reached on whether proximity to faults, soil temperature, or elevation significantly affects microseepage fluxes due to the small size of the data set. A larger data set is necessary to answer such questions that could contribute to the development of an improved microseepage flux model.

There are two further sources of uncertainty in the interpretation of our results that should be mentioned. The first concern is the possibility of measuring contemporaneous biogenic rather than geologic (fossil) methane in positive flux samples. Biogenic methane refers to methane originating from microbial decomposition of organic matter and is common in wetlands and any areas with water-saturated soils (Saunois et al., 2016; Saunois et al., 2020). The two small significantly positive fluxes detected (c1 and j1 in Table S2) were both located near creeks, lakes, or other water sources. Thus, there is potential for the detected small positive fluxes to be the result of biogenic rather than geologic methane emissions, as the flux measurement system used in this study is not capable of distinguishing between the two types of sources.

Second, the flux chamber method measures net CH_4 flux rather than microseepage only. As mentioned above, the soil CH_4 sink is clearly an important process affecting our measurements. A stronger CH_4 soil sink during the warm season has been observed at some temperate forest locations (e.g., Guckland et al., 2009). A seasonally stronger soil CH_4 sink could in principle mask geologic CH_4 emissions. However, our measurements were taken during the fall and winter, with a mean soil temperature of 6.6 °C (median 4.2 °C), while mean annual air temperature in this region is ≈ 9 °C. It therefore seems unlikely that our flux measurements are biased low (with respect to annual

mean flux) by the soil sink. We further note that the soil temperature was above freezing for all measurements, eliminating any concern of frozen soil inhibiting geologic methane release (Table S2).

Conclusions

Our measurements show lower geologic CH_4 microseepage fluxes than most prior data sets. Our results indicate that positive CH_4 microseepage fluxes in Western New York State are not as spatially extensive as previously assumed and that Etiope et al. (2019) very likely overestimated microseepage emissions for this region. However, our study is limited in the number of samples and regional extent and by itself should not be used to evaluate the overall validity of the Etiope et al. (2019) microseepage model.

Continuing measurements at each site would allow for an improved consideration of temporal flux variation, and additional sampling areas would create a more comprehensive look at Western New York State and the Appalachian Basin. In order for improved global estimates of geologic methane microseepage to be developed, and for the Etiope et al. (2019) model to be evaluated, comprehensive sampling needs to take place across a range of different types of hydrocarbon basins, and relationships between microseepage fluxes and proximity to predictive features such as macroseeps and faults need to be quantitatively examined. Any future studies should also include a method to differentiate between geologic and biogenic methane fluxes through measurements of ethane and/or isotopic measurements. We further note that the type of statistical analysis we applied to our data can be used to help guide site selection to maximize the probability of accurately capturing the mean regional fluxes. Finally, future studies of this nature should consider the option of evaluating miniseepage and microseepage as a single category, to avoid any ambiguity involved in distinguishing between these diffuse seepage emission categories.

Data accessibility statement

All data are available in the form of tables in the supplement.

Supplemental files

The supplemental files for this article can be found as follows:

Figure S1. Map of the area of interest in Western New York State. Oil and gas wells (ESOGIS, 2019) with a 1-km radius buffer.

Table S1. Overview of selected sample areas.

Table S2. Field measurements and calculated flux values of every sample taken over the course of this study.

Figure S2. The sampling system setup in the field on November 17, 2019, at Chestnut Ridge Park.

Text S1. Flux chamber testing.

Table S3. Flux chamber volume calibration results.

Figure S3. A schematic of the design for the flux calibration testing. The standard gas tank was switched from a high [CH_4] standard to ultrapure air between positive and negative flux simulations.

Table S4. Flux detection test results.

Figure S4. [CH_4] over the 2.5-h blank test for a sealed intact chamber.

Figure S5. CH_4 concentration over the course of the outdoor blank test (above) and indoor blank test (below).

Figure S6. CH_4 concentration over the course of the breath test (above) and high CH_4 concentration standard gas test (below).

Figure S7. [CH_4] over time for a typical flux chamber sample measurement. This measurement is i – 1 at Watkins Glen State Park on January 9, 2020 (Table S2).

Text S2. Problems encountered during field measurements.

Table S5. Results of a test of the effects of loose quick-connect fitting.

Figure S8. First sample with a time-variable CH_4 trend. [CO_2] (red), [CH_4] (green), and [H_2O] (blue) during sample e-1 at Chestnut Ridge Park on November 17, 2019.

Figure S9. Second sample with a time-variable CH_4 trend. [CO_2] (red), [CH_4] (green), and [H_2O] (blue) during sample e-8 at Chestnut Ridge Park on November 24th, 2019.

Figure S10. Third sample with a time-variable CH_4 trend. [CO_2] (red), [CH_4] (green), and [H_2O] (blue) during sample c-7 at Hemlock Canadice State Forest on January 6th, 2020.

Figure S11. Bar charts of the results. The top left, top right, and bottom-right panels compare average fluxes for sampled areas (areas indicated by letters as in **Figure 2** and Table S1) to Etiope et al. (2019) estimates, with each panel presenting results for a different microseepage emission Level as per Etiope et al. (2019) classification. The bottom-left panel compares average fluxes of each cell Level.

Text S3. Statistical sensitivity testing.

Figure S12. Method for generating synthetic microseepage data sets.

Figure S13. Modes of temporal variability. Time series of microseepage emissions from two distant locations within the same synthetic data set, for cases with (a) asynchronous temporal variability and (b) synchronous temporal variability.

Text S4. Comparison with satellite data from the TROPOMI instrument.

Figure S14. Maps of TROPOMI time-averaged column CH_4 around Etiope et al. (2019) Level 4 cells in Western New York State.

Acknowledgments

We would like to thank Giuseppe Etiope for useful discussions and sharing data, Blair Tinker for guidance with our GIS mapping, Katey Walter-Anthony for sharing her flux chamber design, Christian Frankenberg for helpful discussions about TROPOMI data, Marc Buursink for discussions about Appalachian Basin hydrocarbon reservoirs, and Tolulope Olugboji for discussions about regional and global seismicity. This manuscript was improved by helpful comments from two anonymous referees and from the Editors.

Funding

This work was funded by the David and Lucille Packard Foundation Fellowship for Science and Engineering (to VVP) and NSF Award AGS-2039234 (to VVP and TSW).

Competing interests

The authors have no competing interests to declare.

Author contributions

Contributed to the conception and design: RK and VVP designed the field study.

Contributed to acquisition of data: RK, WS, and VVP conducted the field sampling.

Contributed to analysis and interpretation of data: BH helped to create a preliminary data analysis script. RK expanded this analysis script. TSW conducted the statistical analysis of regional representativeness of the measurements. LTM compiled TROPOMI data. RK, VVP, TSW, and LTM interpreted the data.

Drafted and/or revised the article: RK drafted the article, and VVP, LTM, TSW, and BH provided revisions and guidance.

Approved the submitted version for publication: RK, VVP, WS, LTM, TSW, and BH approved the submitted version for publication.

References

Ciotoli, G, Procesi, M, Etiope, G, Fracassi, U, Ventura, G. 2020. Influence of tectonics on global scale distribution of geological methane emissions. *Nature Communications* **11**(1): 1–8. DOI: http://dx.doi.org/10.1038/s41467-020-16229-1.

Copernicus Sentinel-5P (processed by ESA). 2019. TROPOMI Level 2 Methane total column products. Version 01. European Space Agency. DOI: http://dx.doi.org/10.5270/S5P-3p6lnwd.

Dyonisius, MN, Petrenko, VV, Smith, AM, Hua, Q, Yang, B, Schmitt, J, Beck, J, Seth, B, Bock, M, Hmiel, B, Vimont, I. 2020. Old carbon reservoirs were not important in the deglacial methane budget. *Science* **367**(6480): 907–910. DOI: http://dx.doi.org/10.1126/science.aax0504.

Elder, CD, Thompson, DR, Thorpe, AK, Hanke, P, Walter Anthony, KM, Miller, CE. 2020. Airborne mapping reveals emergent power law of arctic methane emissions. *Geophysical Research Letters* **47**(3). DOI: http://dx.doi.org/10.1029/2019GL085707.

Etiope, G. 2005. Mud volcanoes and microseepage: The forgotten geophysical components of atmospheric methane budget. *Annals of Geophysics* **48**(1). DOI: http://dx.doi.org/10.4401/ag-3175.

Etiope, G. 2015. *Natural gas seepage: The earth's hydrocarbon degassing*. Switzerland: Springer: 199. DOI: http://dx.doi.org/10.1007/978-3-319-14601-0.

Etiope, G, Ciotoli, G, Schwietzke, S, Schoell, M. 2019. Gridded maps of geological methane emissions and their isotopic signature. *Earth System Science Data* **11**: 1–22. DOI: http://dx.doi.org/10.5194/essd-11-1-2019.

Etiope, G, Drobniak, A, Schimmelmann, A. 2013. Natural seepage of shale gas and the origin of "eternal flames" in the Northern Appalachian Basin, USA. *Marine and Petroleum Geology* **43**: 178–186. DOI: http://dx.doi.org/10.1016/j.marpetgeo.2013.02.009.

Etiope, G, Klusman, RW. 2010. Methane microseepage in drylands: Soil is not always a CH4 sink. *Journal of Integrative Environmental Sciences* **7**(S1): 31–38. DOI: http://dx.doi.org/10.1080/19438151003621359.

Etiope, G, Milkov, AV, Derbyshire, E. 2008. Did geologic emissions of methane play any role in quaternary climate change? *Global and Planetary Change* **61**(1–2): 79–88. DOI: http://dx.doi.org/10.1016/j.gloplacha.2007.08.008.

Etiope, G, Nakada, R, Tanaka, K, Yoshida, N. 2011. Gas seepage from Tokamachi mud volcanoes, onshore Niigata Basin (Japan): Origin, post-genetic alterations and CH4–CO2 fluxes. *Applied Geochemistry* **26**(3): 348–359. DOI: http://dx.doi.org/10.1016/j.apgeochem.2010.12.008.

Etiope, G, Papatheodorou, G, Christodoulou, DP, Ferentinos, G, Sokos, E, Favali, P. 2006. Methane and hydrogen sulfide seepage in the northwest Peloponnesus petroliferous basin (Greece): Origin and geohazard. *AAPG Bulletin* **90**(5): 701–713. DOI: http://dx.doi.org/10.1306/11170505089.

Etiope, G, Schwietzke, S. 2019. Global geological methane emissions: An update of top-down and bottom-up estimates. *Elementa Science of the Anthropocene* **47**(7): 1–9. DOI: http://dx.doi.org/10.1525/elementa.383.

Etminan, M, Myhre, G, Highwood, EJ, Shine, KP. 2016. Radiative forcing of carbon dioxide, methane, and nitrous oxide: A significant revision of the methane radiative forcing. *Geophysical Research Letters* **43**(24): 12–614. DOI: http://dx.doi.org/10.1002/2016GL071930.

Fountain, JC, Jacobi, RD. 2000. Detection of buried faults and fractures using soil gas analysis. *Environmental & Engineering Geoscience* **6**(3): 201–208. DOI: http://dx.doi.org/10.2113/gseegeosci.6.3.201.

Guckland, A, Flessa, H, Prenzel, J. 2009. Controls of temporal and spatial variability of methane uptake in soils of a temperate deciduous forest with different abundance of European beech (Fagus sylvatica L.). *Soil Biology and Biochemistry* **41**(8): 1659–1667. DOI: http://dx.doi.org/10.1016/j.soilbio.2009.05.006.

Hmiel, B, Petrenko, VV, Dyonisius, MN, Buizert, C, Smith, AM, Place, PF, Harth, C, Beaudette, R, Hua, Q, Yang, B, Vimont, I. 2020. Preindustrial $^{14}CH_4$ indicates greater anthropogenic fossil CH_4 emissions. *Nature* **578**(7795): 409–412. DOI: http://dx.doi.org/10.1038/s41586-020-1991-8.

Hu, H, Landgraf, J, Detmers, R, Borsdorff, T, Aan de Brugh, J, Aben, I, Butz, A, Hasekamp, O. 2018. Toward global mapping of methane with TROPOMI: First results and intersatellite comparison to GOSAT. *Geophysical Research Letters* **45**(8): 3682–3689. DOI: http://dx.doi.org/10.1002/2018GL077259.

Incorporated Research Institutions for Seismology (IRIS), Global Seismographic Network. 2021. Jumbo Seismic Monitor. Available at http://ds.iris.

edu/seismon/bigmap/index.phtml. Accessed 1 March 2021.

Isachsen, YW, McKendree, WG. 1977. Preliminary brittle structure map of New York, scale 1: 250,000. *NY State Museum Science Service Map Chart Series* **31**. Available at http://www.nysm.nysed.gov/research-collections/geology/gis. Accessed 21 August 2019.

Jacobi, RD. 2002. Basement faults and seismicity in the Appalachian Basin of New York State. *Tectonophysics* **353**(1–4): 75–113. DOI: http://dx.doi.org/10.1016/S0040-1951(02)00278-0.

Klusman, RW. 2003. Rate measurements and detection of gas microseepage to the atmosphere from an enhanced oil recovery/sequestration project, Rangely, Colorado, USA. *Applied Geochemistry* **18**(12): 1825–1838. DOI: http://dx.doi.org/10.1016/S0883-2927(03)00108-2.

Klusman, RW. 2005. Baseline studies of surface gas exchange and soil-gas composition in preparation for CO2 sequestration research: Teapot Dome, Wyoming. *AAPG Bulletin* **89**(8): 981–1003. DOI: http://dx.doi.org/10.1306/03310504109.

Klusman, RW, Leopold, ME, LeRoy, MP. 2000. Seasonal variation in methane fluxes from sedimentary basins to the atmosphere: Results from chamber measurements and modeling of transport from deep sources. *Journal of Geophysical Research: Atmospheres* **105**(D20): 24661–24670. DOI: http://dx.doi.org/10.1029/2000JD900407.

LT Environmental, Inc. 2007. *Phase II Raton Basin gas seep investigation; Las Animas and Huerfano counties*. Colorado: Oil and gas conservation response fund. Project #1925. Available at http://cogcc.state.co.us/Library/Ratoasin/Phase%20II%20Seep%20Investigation%20Final%20Report.pdf.

Nicewonger, MR, Verhulst, KR, Aydin, M, Saltzman, ES. 2016. Preindustrial atmospheric ethane levels inferred from polar ice cores: A constraint on the geologic sources of atmospheric ethane and methane. *Geophysical Research Letters* **43**(1): 214–221. DOI: http://dx.doi.org/10.1002/2015GL066854.

Oertel, C, Matschullat, J, Zurba, K, Zimmermann, F, Erasmi, S. 2016. Greenhouse gas emissions from soils—A review. *Geochemistry* **76**(3): 327–352. DOI: http://dx.doi.org/10.1016/j.chemer.2016.04.002.

Petrenko, VV, Smith, AM, Schaefer, H, Riedel, K, Brook, E, Baggenstos, D, Harth, C, Hua, Q, Buizert, C, Schilt, A, Fain, X. 2017. Minimal geological methane emissions during the Younger Dryas–Preboreal abrupt warming event. *Nature* **548**(7668): 443–446. DOI: http://dx.doi.org/10.1038/nature23316.

Ryder, RT. 2008, Assessment of Appalachian basin oil and gas resources: Utica-Lower Paleozoic Total Petroleum System. U.S. Geological Survey Open-File Report 2008–1287. DOI: http://dx.doi.org/10.3133/ofr20081287.

Saunois, M, Bousquet, P, Poulter, B, Peregon, A, Ciais, P, Canadell, JG, Dlugokencky, EJ, Etiope, G, Bastviken, D, Houweling, S, Janssens-Maenhout, G. 2016. The global methane budget 2000–2012. *Earth System Science Data* **8**(2): 697–751. DOI: http://dx.doi.org/10.5194/essd-8-697-2016.

Saunois, M, Stavert, AR, Poulter, B, Bousquet, P, Canadell, JG, Jackson, RB, Raymond, PA, Dlugokencky, EJ, Houweling, S, Patra, PK, Ciais, P. 2020. The global methane budget 2000–2017. *Earth System Science Data* **12**(3): 1561–1623. DOI: http://dx.doi.org/10.5194/essd-12-1561-2020.

Schimmelmann, A, Ensminger, SA, Drobniak, A, Mastalerz, M, Etiope, G, Jacobi, RD, Frankenberg, C. 2018. Natural geological seepage of hydrocarbon gas in the Appalachian Basin and Midwest USA in relation to shale tectonic fracturing and past industrial hydrocarbon production. *Science of the Total Environment* **644**: 982–993. DOI: http://dx.doi.org/10.1016/j.scitotenv.2018.06.374.

Schulte, SM, Mooney, WD. 2005. An updated global earthquake catalogue for stable continental regions: Reassessing the correlation with ancient rifts. *Geophysical Journal International* **161**(3): 707–721. DOI: http://dx.doi.org/10.1111/j.1365-246X.2005.02554.x.

Schwietzke, S, Sherwood, OA, Bruhwiler, LM, Miller, JB, Etiope, G, Dlugokencky, EJ, Michel, SE, Arling, VA, Vaughn, BH, White, JW, Tans, PP. 2016. Upward revision of global fossil fuel methane emissions based on isotope database. *Nature* **538**(7623): 88–91. DOI: http://dx.doi.org/10.1038/nature19797.

Sciarra, A, Cinti, D, Pizzino, L, Procesi, M, Voltattorni, N, Mecozzi, S, Quattrocchi, F. 2013. Geochemistry of shallow aquifers and soil gas surveys in a feasibility study at the Rivara natural gas storage site (Po Plain, Northern Italy). *Applied Geochemistry* **34**: 3–22. DOI: http://dx.doi.org/10.1016/j.apgeochem.2012.11.008.

Tang, J, Bao, Z, Xiang, W, Gou, Q. 2007. Daily variation of natural emission of methane to the atmosphere and source identification in the Luntai fault region of the Yakela condensed oil/gas field in the Tarim Basin, Xinjiang, China. *Acta Geologica Sinica-English Edition* **81**(5): 771–778. DOI: http://dx.doi.org/10.1111/j.1755-6724.2007.tb01001.x.

Tang, J, Xu, Y, Wang, G, Etiope, G, Han, W, Yao, Z, Huang, J. 2017. Microseepage of methane to the atmosphere from the Dawanqi oil-gas field, Tarim Basin, China. *Journal of Geophysical Research: Atmospheres* **122**(8): 4353–4363. DOI: http://dx.doi.org/10.1002/2016JD026385.

Tang, J, Yin, H, Wang, G, Chen, Y. 2010. Methane microseepage from different sectors of the Yakela condensed gas field in Tarim Basin, Xinjiang, China. *Applied Geochemistry* **25**(8): 1257–1264. DOI: http://dx.doi.org/10.1016/j.apgeochem.2010.05.011.

U.S. Geological Survey (USGS), NEIC PDE Catalog, National Earthquake Information Center. Available at https://www.usgs.gov/natural-hazards/earthquake-hazards/earthquakes. Accessed 21 August 2019.

How to cite this article: Kazemi, R, Schlageter, W, Hmiel, B, Weber, TS, Murray, LT, Petrenko, VV. 2021. Investigating methane emissions from geologic microseepage in Western New York State, United States. *Elementa: Science of the Anthropocene* 9(1). DOI: https://doi.org/10.1525/elementa.2020.00066

Domain Editor-in-Chief: Detlev Helmig, Boulder AIR LLC, Boulder, CO, USA

Associate Editor: Lori Bruhwiler, National Oceanic & Atmospheric Administration, Earth System Research Laboratory, Global Monitoring Division, Boulder, CO, USA

Knowledge Domain: Atmospheric Science

Published: May 26, 2021 **Accepted:** April 26, 2021 **Submitted:** June 8, 2020

ELEMENTA Science of the Anthropocene

Elem Sci Anth is a peer-reviewed open access journal published by University of California Press.

OPEN ACCESS